Chinese Journal of Natural Medicines

Discovery of proqodine A derivatives with antitumor activity targeting NAD(P)H: quinone oxidoreductase 1 and nicotinamide phosphoribosyltransferase

Jiangzhou SONG, Guiqing ZOU, Zhou ZHAO, Ya ZHU, Jiayu XUE, Lanjia AO, Huiyong SUN, Haiping HAO, Bo ZHANG, Xiaowei XU

Citation: Jiangzhou SONG, Guiqing ZOU, Zhou ZHAO, Ya ZHU, Jiayu XUE, Lanjia AO, Huiyong SUN, Haiping HAO, Bo ZHANG, Xiaowei XU, Discovery of proqodine A derivatives with antitumor activity targeting NAD(P)H: quinone oxidoreductase 1 and nicotinamide phosphoribosyltransferase, Chinese Journal of Natural Medicines, 2024, 22(1), 75−88. doi: 10.1016/S1875−5364(24)60564−9.

View online: https://doi.org/10.1016/S1875−5364(24)60564−9

Available online at www.sciencedirect.com
ScienceDirect
Chinese Journal of Natural Medicines 2024, **22**(1): 75-88
doi: 10.1016/S1875-5364(24)60564-9
Chinese Journal of Natural Medicines

•Original article•

Discovery of proqodine A derivatives with antitumor activity targeting NAD(P)H: quinone oxidoreductase 1 and nicotinamide phosphoribosyltransferase

SONG Jiangzhou[1Δ], ZOU Guiqing[1, 2Δ], ZHAO Zhou[1], ZHU Ya[1], XUE Jiayu[1], AO Lanjia[1], SUN Huiyong[1], HAO Haiping[1*], ZHANG Bo[2*], XU Xiaowei[1*]

[1] *State Key Laboratory of Natural Medicines, Key Lab of Drug Metabolism and Pharmacokinetics, China Pharmaceutical University, Nanjing 210009, China;*
[2] *State Key Laboratory of Natural Medicines, China Pharmaceutical University, Nanjing 210009, China*

Available online 20 Jan., 2024

[ABSTRACT] NAD(P)H: quinone oxidoreductase 1 (NQO1) is a flavin protease highly expressed in various cancer cells. NQO1 catalyzes a futile redox cycle in substrates, leading to substantial reactive oxygen species (ROS) production. This ROS generation results in extensive DNA damage and elevated poly (ADP-ribose) polymerase 1 (PARP1)-mediated consumption of nicotinamide adenine dinucleotide (NAD^+), ultimately causing cell death. Nicotinamide phosphoribosyltransferase (NAMPT), the rate-limiting enzyme in the NAD^+ salvage synthesis pathway, emerges as a critical target in cancer therapy. The concurrent inhibition of NQO1 and NAMPT triggers hyperactivation of PARP1 and intensive NAD^+ depletion. In this study, we designed, synthesized, and assessed a novel series of proqodine A derivatives targeting both NQO1 and NAMPT. Among these, compound **T8** demonstrated potent antitumor properties. Specifically, **T8** selectively inhibited the proliferation of MCF-7 cells and induced apoptosis through mechanisms dependent on both NQO1 and NAMPT. This discovery offers a promising new molecular entity for advancing anticancer research.

[KEY WORDS] NQO1; ROS; NAMPT; NAD^+; T8
[CLC Number] R284, R965 **[Document code]** A **[Article ID]** 2095-6975(2024)01-0075-14

Introduction

The evolution of tumor biology and multi-omics has significantly enhanced our understanding of the molecular mechanisms underlying tumor development and progression. Hanahan and Weinberg have characterized the nature of tumors through six biological capabilities: sustaining proliferative signaling, resisting cell death, inducing angiogenesis, enabling replicative immortality, activating invasion and metastasis, and evading growth suppressors [1]. In addition, they proposed four other important characteristics, one of which is the abnormal energy metabolism of tumor cell lines [2]. At present, targeting overexpressed metabolic enzymes in tumors has become a promising approach in cancer therapy, and the metabolism of nicotinamide adenine dinucleotide (NAD^+) has received mounting attention [3-6]. NAD(P)H: quinone oxidoreductase 1 (NQO1) is a flavin protease that catalyzes a two-electron reduction of various quinones directly to the hydroquinone by utilizing NAD(P)H as a cofactor [7-11]. NQO1 catalysis induces a two-electron redox cycle, generating unstable hydroquinones that rapidly revert to semiquinones or quinones. This futile cycle leads to NAD(P)H oxidation and elevated reactive oxygen species (ROS) levels, causing DNA damage, hyperactivation of PARP1, NAD^+ depletion, and consequent tumor cell death (Fig. 1) [7, 9, 12-18]. NQO1 is highly expressed in most solid cancers, making it a potential therapeutic target for selectively eliminating cancer cells with minimal toxicity to normal cells [19-21]. Representative NQO1 substrates include deoxynyboquinone (DNQ) [22], *β*-lapachone (*β*-lap) [9], and pronqodine A (Fig. 2A) [23].

As the rate-limiting enzyme of the NAD^+ salvage synthesis pathway, NAMPT converts nicotinamide (NAM) to nicotinamide mononucleotide (NMN), which plays an im-

[Received on] 12-Aug.-2023
[Research funding] This work was supported by the National Key Research and Development Programme of China (No. YFA1303800), the Fundamental Research Funds for the Central Universities (No. 2632023TD10) and the National Natural Science Foundation of China (No. 81930109).
[*]**Corresponding author]** E-mails: haipinghao@cpu.edu.cn (HAO Haiping); zb3981444@cpu.edu.cn (ZHANG Bo); xw@cpu.edu.cn (XU Xiaowei)
[Δ]These authors contributed equally to this work.
These authors have no conflict of interest to declare.

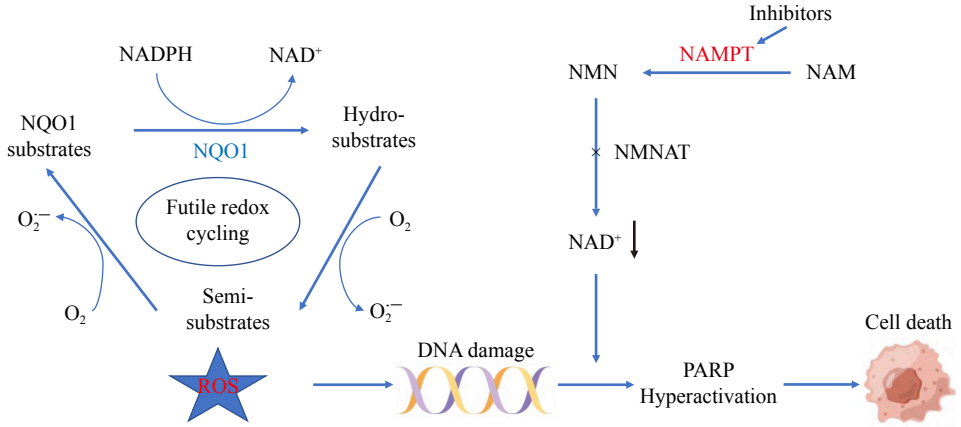

Fig. 1 The synergistic antitumor mechanism of NQO1 substrate and nicotinamide phosphoribosyltransferase (NAMPT) inhibitors. NQO1 substrates undergo a futile redox cycle by NQO1. These redox reactions produce large quantities of ROS, which result in DNA damage, hyperactivation of PARP1, depletion of NAD^+ and ATP, and ultimately cell death.

portant role in NAD metabolism [24, 25]. Indeed, NAMPT inhibitors, including FK866, TRON-8, and GWX1777, have shown potential (Fig. 2B) [15]. Research has indicated that combining NQO1 substrates with different drugs, particularly NAMPT inhibitors, can significantly deplete intracellular NAD^+ and enhance tumor cell apoptosis due to their complementary mechanisms [15, 18]. For example, combining the NQO1 substrate Tanshinone IIA with FK866 resulted in a more severe depletion of NAD^+ [26]. Compared with FK866 treatment alone, co-treatment with *β*-lap can achieve synergistic anticancer efficacy, allowing for lower doses and shorter treatment time and compensating for the lack of antitumor selectivity for FK866 as the single agent [15]. Therefore, we envisaged whether the NQO1 substrate and the key pharmacophore of the NAMPT inhibitor can be integrated into a novel dual-target molecule [27]. This molecule could produce toxic ROS *via* NQO1-catalyzed redox cycling, causing direct DNA damage to tumor cells, while inhibiting NAMPT activity and impairing DNA repair by PARP1, ultimately inducing tumor cell death. Thus, we designed, synthesized, and evaluated a series of new dual-target compounds targeting NQO1 and NAMPT. We selected pronqodine A for its simplicity and ease of synthesis as a lead compound [23]. We then combined it with key pharmacophores from NAMPT inhibitors FK866 [28-30], TRON-8 [31], and GMX1778 [32-35] to construct a series of novel dual-target compounds together with pronqodine A. Among these, compound **T8** exhibited potent antitumor activity.

Results and Discussion

Design and synthesis of a series of dual-target compounds

We intend to select a promising NQO1 substrate for

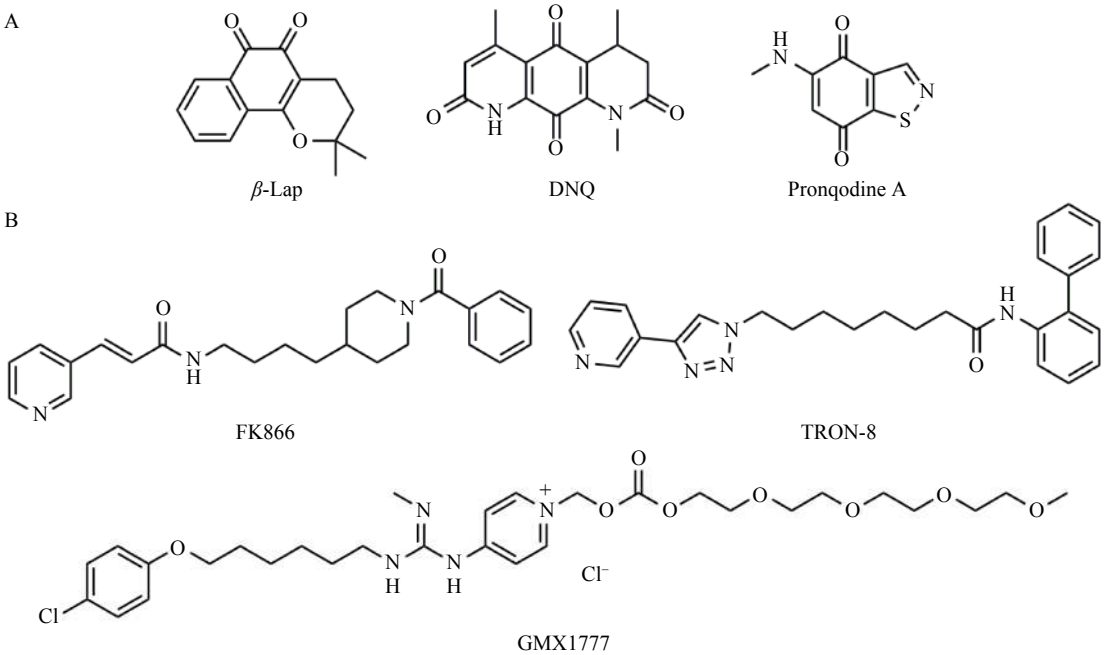

Fig. 2 Reported (A) NQO1 substrates and (B) NAMPT inhibitors.

modification, analyze the key pharmacophore of the reported NAMPT inhibitors, and then design a rational synthetic route to combine them into a dual-target molecule by a suitable linker. We reviewed various NQO1 substrates reported in the literature, focusing on those that are both extensively studied and relatively easy to synthesize, such as *β*-lap, DNQ, and pronqodine A (Fig. 1A). Our experiments revealed challenges with these substrates: the pyran ring in *β*-lap exhibited poor stability and difficulty in attaching a side chain linker; DNQ proved challenging for introducing functional groups like amino or carboxyl groups for linkage; pronqodine A, however, with its isothiazolo-benzoquinone bicyclic structure, emerged as a promising template for modification. The Moody group's synthetic route for pronqodine A, starting from 2,5-dimethoxybenzaldehyde was particularly instructive [36]. The final step in their synthesis, involving an addition-elimination reaction of a free amino group with quinone under cerium chloride catalysis, indicated a feasible approach for incorporating the amino group at the end of the NAMPT inhibitor's key pharmacophore into the isothiazolobenzoquinone structure of pronqodine A to yield dual-target molecules. Consequently, we selected pronqodine A as our lead compound and used it as the template to bind the key pharmacophore of NAMPT inhibitors. Several representative NAMPT inhibitors, including FK866, TRON-8, and GMX1778 (prodrug GMX1777), feature longer carbon chain linkers, facilitating the modification of the amino structure at their ends (Fig. 1B). We chose the active pyridine side of these NAMPT inhibitors and introduced a carbon chain with a free amino group at the end, reacting it with isothiazolobenzoquinone under cerium chloride catalysis to synthesize dual-target molecules (Fig. 3).

Based on the above analysis, a series of target compounds were designed and finally synthesized. 1,2-Benzisothiazole-4,7-dione was synthesized *as per* the previously reported method [36]. The target compound **P2** was synthesized according to the procedure in Scheme 1. By Mitsunobu reaction, the hydroxyl functional group of tert-butyl 4-(4-hydroxybutyl) piperidine-1-carboxylate (**2**) was replaced by the amino group of phthalimide, yielding intermediate **3**. The primary amine (**4**) was obtained by hydrolysis of hydrazine hydrate. The 3-pyridineacrylic acid was transformed into an acyl chloride intermediate under the thionyl chloride and subsequently reacted with compound **4** to form an amide. Compound **6** was then reacted with 1,2-benzisothiazole-4,7-dione to produce **P2** through an addition-elimination mechanism. **P3**−**P8** were synthesized according to the procedure in Scheme 2, which was similar to compound **P2**. The synthetic pathways for **T5**−**T8** are illustrated in Scheme 3. The commercially available 3-ethynylpyridine was reacted with the proper azide alcohols (**12a**−**12d**), obtained for azidation of the commercially available bromo derivative (**11a**−**11d**), using the Click reaction to yield the triazole intermediates (**13a**−**13d**). The hydroxyl functional group was converted into azide (**14a**−**14d**) with DPPA, DBU, and sodium azide. Azides **14a**−**14d** were reduced to amines **15a**−**15d** using the Staudinger reaction. Similarly, compounds **15a**−**15d** were reacted with 1,2-benzisothiazole-4,7-dione to yield **T5**−**T8** under the catalysis of cerium chloride.

In vitro evaluation of antitumor activity of compounds

To assess the antitumor activity of the series of compounds, we first conducted a qualitative analysis of NQO1 and NAMPT enzyme levels in two cancer cell lines: A549 (non-small-cell lung cancer cell line, NSCLC) and MCF-7 (human breast cancer cell line, HBC) by Western blotting. The results confirmed the high expressions of NQO1 and NAMPT proteins in both A549 and MCF-7 cells (Fig. S1). The primary assessment of the compounds' antitumor activity was performed using the sulforhodamine B (SRB) assay in A549 and MCF-7 cells [37]. The SRB dye specifically binds to the basic amino acid of the protein in cellular proteins, yielding an absorption peak at 515 nm. The absorbance is directly proportional to the quantity of living cells, thus providing an indirect measure of the compounds' antitumor efficacy. As depicted in Table 1, the results showed that the IC_{50} values for most compounds against A549 and MCF-7 cells were in the micromolar range, and the antitumor activity of compounds **T5**−**T8** was enhanced compared with that of compounds **P3**−**P8**, indicating a significant impact of the triazole ring on activity. Notably, **T5** and **T8** exhibited the

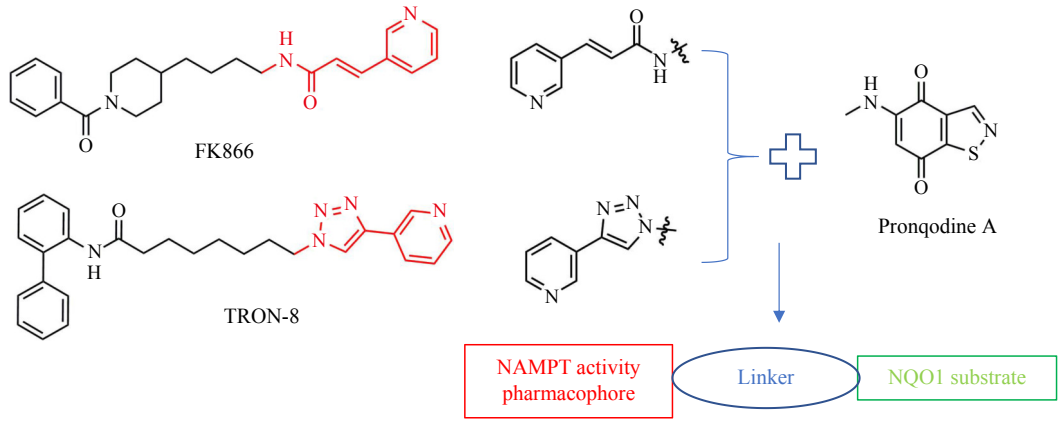

Fig. 3 Design strategy of the small molecules targeting NQO1 and NAMPT.

highest antitumor activity against MCF-7 and A549 cells, respectively (Table 1). These findings indicate that the compounds we designed and synthesized possess discernible antitumor activity, warranting further research.

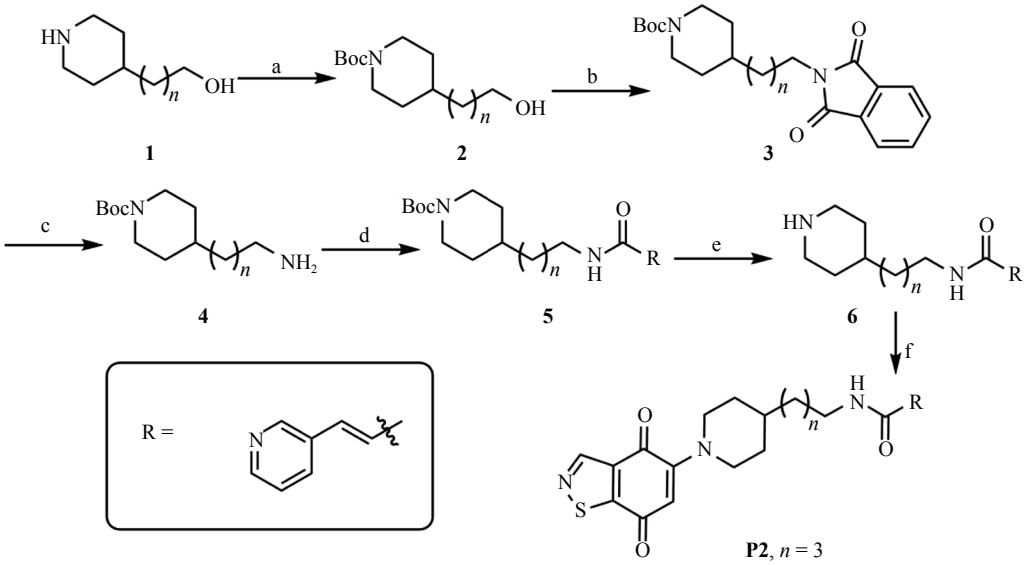

Scheme 1 Synthesis of compound P2. Reagents and conditions: (a) Boc_2O, THF/H_2O, RT, 12 h; (b) phthalimide, PPh_3, DEAD, THF, RT, 16 h; (c) hydrazine hydrate, EtOH, reflux, 4 h; (d) 3-pyridineacrylic acid, thionyl chloride, CH_2Cl_2, 2 h then DIEA, RT, 12 h; (e) HCl 2 mol·L^{-1} in EtOH, 0 °C, 12 h; (f) 1,2-benzisothiazole-4,7-dione, cerium (III) chloride, DIEA, EtOH, RT, 5 h.

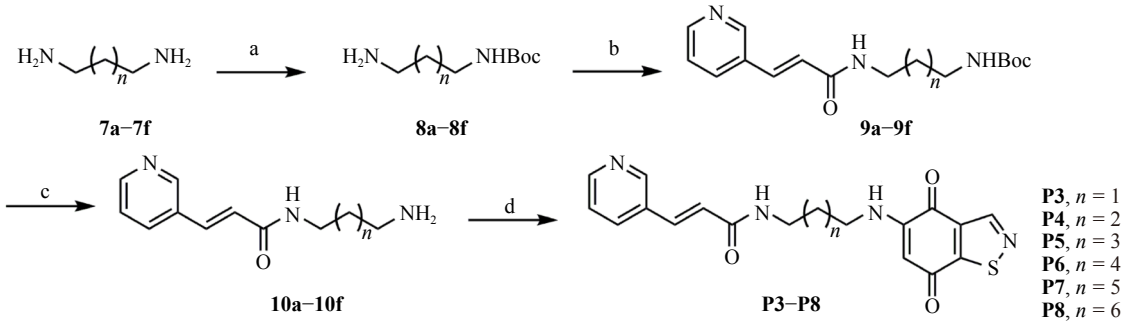

Scheme 2 Synthesis of compounds P3–P8. Reagents and conditions: (a) Boc_2O, THF/H_2O, RT, 12 h; (b) 3-pyridineacrylic acid, thionyl chloride, CH_2Cl_2, 2 h then DIEA, RT, 12 h; (c) HCl 2 mol·L^{-1} in EtOH, 0 °C,12 h; and (d) 1,2-benzisothiazole-4,7-dione, cerium (III) chloride, DIEA, EtOH, RT, 5 h.

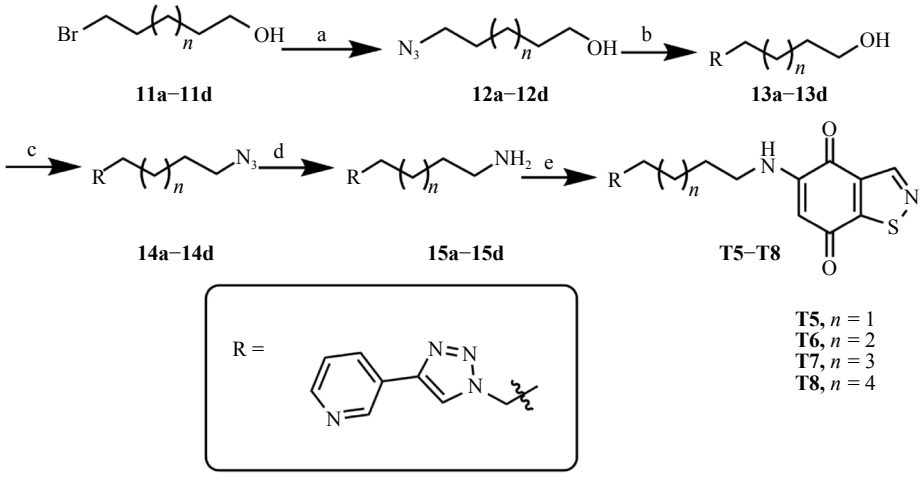

Scheme 3 Synthesis of compounds T5–T8. Reagents and conditions: (a) NaN_3, 80 °C, 2 h; (b) 3-ethynylpyridine, $CuSO_4·5H_2O$, sodium ascorbate, *t*-BuOH/H_2O, 40 °C, 12 h; (c) DPPA, DBU, 25 °C, 0.5 h then NaN_3, 3 h; (d) PPh_3, H_2O, THF, reflux, 3 h; and (e) 1,2-benzisothiazole-4,7-dione, cerium (III) chloride, DIEA, EtOH, RT, 5 h.

Table 1 *In vitro* antiproliferative activity (IC_{50}) of compounds against NSCLC A549 and HBC MCF-7 cells (mean ± SD, *n* = 6/group).

Compd	A549 IC_{50}/(μmol·L^{-1})	MCF-7 IC_{50}/(μmol·L^{-1})
P2	> 20	12.19 ± 1.10
P3	12.39 ± 1.34	1.25 ± 1.16
P4	17.14 ± 1.18	4.55 ± 1.11
P5	7.02 ± 1.16	3.88 ± 1.32
P6	> 20	6.69 ± 1.03
P7	12.46 ± 1.17	1.94 ± 1.19
P8	14.95 ± 1.31	11.43 ± 1.30
T5	1.82 ± 1.11	2.54 ± 1.24
T6	1.47 ± 1.27	3.83 ± 1.17
T7	1.52 ± 1.30	3.13 ± 1.13
T8	1.39 ± 1.40	4.59 ± 1.42

Antitumor activity was assessed using the SRB assay.

In vitro evaluation of the antitumor activity of compounds against NQO1$^{(+/-)}$ MDA-MB-231 cells

To elucidate the NQO1 dependency of our compounds' anticancer activity, we used the human breast cancer cell line MDA-MB-231, known for its low NQO1 expression, as a model. We engineered an NQO1-overexpressing variant of this cell line using NQO1 lentivirus (LV) infection. Our objective was to confirm the successful construction of NQO1 overexpressing cells and to investigate whether the antitumor activity of our compounds is indeed dependent on NQO1 expression. As shown in Fig. 4A, MDA-MB-231 (NQO1^{+}) cells infected with LV-NQO1 successfully expressed NQO1 protein, while MDA-MB-231 (NQO1^{-}) cells (the control group) did not show NQO1 expression. Notably, NAMPT protein levels remained consistent in both MDA-MB-231 (NQO1$^{+/-}$) cell variants, indicating that LV infection has no effect on the original NAMPT in these cells.

We then employed the SRB assay to assess the inhibitory activity of the compounds in MDA-MB-231 (NQO1$^{+/-}$) cells. The results revealed that the IC_{50} values of these compounds in MDA-MB-231 (NQO1^{+}) cells were predominantly in the micromolar range, and the antitumor activity was significantly increased compared with that of MDA-MB-231 (NQO1^{-}) cells. In particular, the compounds **T5**−**T8** exhibited superior anticancer activity in the MDA-MB-231 (NQO1^{+}) compared with the compounds **P2**−**P8**. Notably, compound **T8** showed the highest anticancer activity in MDA-MB-231 (NQO1^{+}) cells (Table 2), suggesting that its antitumor activity is NQO1-dependent. Given compound **T8**'s promising *in vitro* anticancer activity, it was selected for further research and exploration.

To investigate **T8**'s function as an NQO1 substrate, we monitored the depletion of NAD(P)H, an electron donor for NQO1 that absorbs strongly at 340 nm (its oxidized form NAD^+ has minimal absorption at this wavelength). The gradual decrease in NAD(P)H absorbance at 340 nm, observed with compound **T8** and also with pronqodine A (Fig. 4B), confirmed significant NAD(P)H depletion. This result validated compound **T8** as an effective NQO1 substrate.

In vitro inhibitory activity of compound T8 against NAMPT

To evaluate compound **T8**'s inhibitory activity against NAMPT, we used the CycLex NAMPT Inhibitor Screening Kit, MBL [38]. The representative NAMPT inhibitor FK866 exhibited an IC_{50} value of 96.7 nmol·L^{-1}. The results revealed that compound **T8** (IC_{50} 404.1 nmol·L^{-1}) is a NAMPT inhibitor, possessing NAMPT inhibitory activity (Fig. S2). Further investigation into the biological impact of **T8**'s NAMPT inhibitory activity was conducted by measuring cellular NAD^+ levels in A549 cells using a NAD^+ test kit. As shown in Fig. 4C, the level of cellular NAD^+ showed a downtrend with the prolongation of **T8** (10 μmol·L^{-1}) treatment. This trend indicates that **T8** effectively reduces NAD^+ levels in cells, a likely consequence of its NAMPT inhibitory activity.

In vitro cell selectivity of compound T8

The evaluation of compound **T8**'s selectivity between cancer and normal cells is a critical aspect of its therapeutic

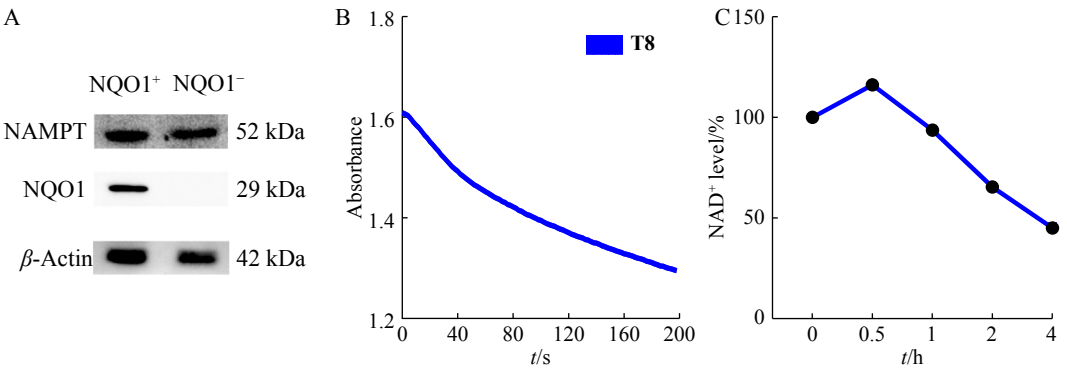

Fig. 4 Compound T8 reduced the cellular NAD^+ content in a time-dependent manner. (A) Western blotting analysis of NQO1$^{(+)}$ and NQO1$^{(-)}$ MDA-MB-231 cells. (B) Under the catalysis of NQO1, the absorbance of NAD(P)H at 340 nm gradually decreased after treatment with T8 (20 μmol·L^{-1}). (C) The level of cellular NAD^+ after treatment with T8 (10 μmol·L^{-1}) was tested by the NAD^+ test kit in A549 cells.

Table 2 *In vitro* antitumor activity of compound T8 in an NQO1-dependent manner in NQO1$^{(+)}$ and NQO1$^{(-)}$ MDA-MB-231 cells (mean ± SD, *n* = 6/group)

Compd	NQO1$^{(+)}$ IC_{50}/(μmol·L^{-1})	NQO1$^{(-)}$ IC_{50}/(μmol·L^{-1})
P2	9.9	6.3
P3	12.37 ± 2.44	> 20
P4	6.60 ± 1.30	> 20
P5	3.07 ± 1.36	> 20
P6	8.48 ± 1.47	> 20
P7	3.31 ± 2.44	7.2
P8	4.49 ± 1.25	> 20
T5	1.25 ± 1.10	> 10
T6	1.55 ± 1.06	> 20
T7	1.48 ± 1.19	> 20
T8	0.92 ± 1.06	> 20

Antitumor activity was assessed using the SRB assay.

potential. While its potent antitumor activity *in vitro* is promising, understanding its toxicity profile, especially in non-cancerous cells, is essential for assessing its viability as a cancer treatment. For this purpose, we chose NQO1-rich and NAMPT-expressing MCF-7 cells (human breast cancer cells) as our cancer cell model. To assess the selectivity of compound **T8**, we compared its effects on MCF-7 cells with its effects on normal hepatic cells (L02) and AML-12 cells (a mouse hepatocyte cell line) using the Cell Counting Kit-8 (CCK-8) assay. The results revealed that compound **T8** exhibited significant antitumor activity against MCF-7 cells (IC_{50} 0.107 μmol·L^{-1}). NQO1-deficient normal L02 cells (IC_{50} 2.466 μmol·L^{-1}) and AML-12 cells (IC_{50} 5.444 μmol·L^{-1}) were much less sensitive to compound **T8**, suggesting that compound **T8** possesses good selectivity between cancer cells and normal cells (Figs. 5A−5C). Moreover, compound **T8** exhibited high selectivity toward cancer cells over normal L02 cells (selectivity ratio = 50.88) and normal AML-12 cells (selectivity ratio = 23.05) (Fig. 5D). Additionally, when comparing the antitumor activity of compound **T8** with the known NAMPT inhibitor FK866, compound **T8** demonstrated more effective antitumor activity (Fig. S3).

Compound T8 exhibited antitumor activity in a NQO1- and NAMPT-dependent manner

In order to further determine whether the antitumor activity of compound **T8** was dependent on NQO1 and NAMPT, we co-incubated MCF-7 cells with compound **T8** and NAC (1 mmol·L^{-1}) or NMN (200 μmol·L^{-1}) for 24 h. CCK-8 assay results showed that NAC and NMN remarkably diminish the inhibition of compound **T8** on the proliferation of MCF-7 cells (Figs. 6A and 6B). These results indicate that compound **T8** exerts its antitumor activity against MCF-7 cells in an NQO1-and NAMPT-dependent manner.

Identification of cancer cell death mode induced by compound T8

ROS levels in MCF-7 cells were measured using the DCFH-DA probe. As shown in Fig. 7A, treatment with compound **T8** led to a concentration-dependent increase in cellular ROS levels in MCF-7 cells. MCF-7 cells were separately cultured with **T8** (20 μmol·L^{-1}, 10 h), **T8** (20 μmol·L^{-1}, 10 h) + DIC (5 mmol·L^{-1}, 6 h), **T8** (20 μmol·L^{-1}, 10 h) + NAC (5 mmol·L^{-1}, 6 h), and negative control. The fluorescence intensity was enhanced in MCF-7 cells treated with **T8** + DIC/NAC compared with that in cells received other treatments (Fig. 7B). These results showed that compound **T8**

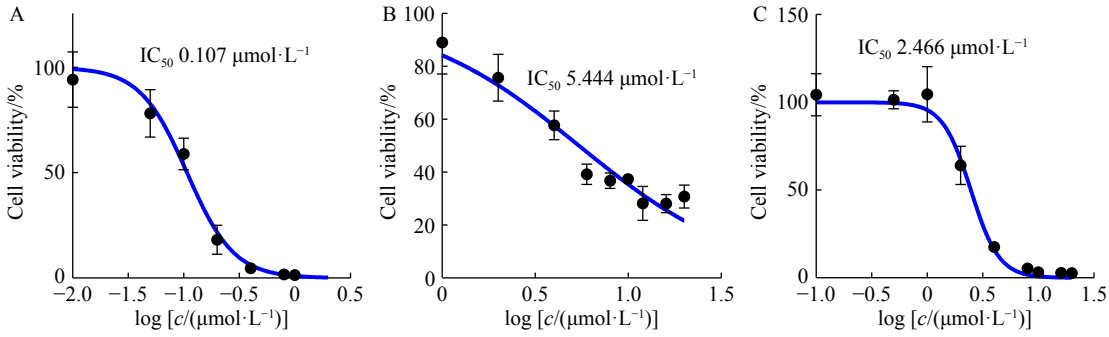

D

Compd	IC_{50}/(μmol·L^{-1}) MCF-7	AML-12	L02	IC_{50} value ratio AML-12/MCF-7	L02/MCF-7
T8	0.107 ± 0.01	5.444 ± 0.562	2.466 ± 0.196	50.88	23.05

Fig. 5 Compound T8 exhibited selectivity toward cancer cells over normal cells. IC_{50} of (A) MCF-7, (B) AML-12, and (C) L02 cells were tested by the CCK-8 assay. (D) Selectivity ratio of AML-12 and L02 cells to MCF-7 cells. MCF-7 was used as the positive control. MCF-7 cells were treated with different concentrations of compound T8 for 24 h. Subsequently, the antiproliferative activity was assessed by the CCK8 assay. Data are presented as the mean ± SD (*n* = 6/group). For each representative IC_{50} value, three independent experiments were performed.

generated ROS in MCF-7 cells, and DIC and NAC led to a significant decrease in ROS generation, suggesting that **T8**'s mechanism involves ROS-mediated pathways. Therefore, flow cytometry was performed to identify the cell death mode induced by compound **T8**. MCF-7 cells were treated with the different concentrations (L-G, 0.04 μmol·L^{-1}; M-G, 0.08 μmol·L^{-1}; H-G, 0.1 μmol·L^{-1}) of compound **T8** for 24 h using AV/PI staining. Compound **T8** significantly induced cell apoptosis in a concentration-dependent manner (Figs. 8A and 8B). In summary, compound **T8** induces cell apoptosis by elevating ROS levels.

Binding modes of compound T8 to NQO1 and NAMPT

In 1999, the structure of NQO1 was first analyzed, providing an important reference for structure-based drug design [39]. The catalytically active domain of NQO1 is a flexible binding pocket with hydrophobic properties, which provides an important structural biological basis for the catalysis of quinone substrates with rigid planar structures. To understand the binding mode of compound **T8** to NQO1, the atomic coordinates of the crystal structure of NQO1 (PDB code 2F1O) have been used for docking. As shown in Fig. 9A, the benzoquinone structure of **T8** was embedded in the catalytic domain of NQO1. It formed hydrogen bonds with adjacent Tyr127, Tyr129, Phe179, and Trp107 residues, while the NAMPT pharmacophore moiety extended to the solvent area of the NQO1 protein. Then, we used the crystal structure of NAMPT (PDB code 2GVJ) to explore how compound **T8** interacts with this enzyme. The molecular docking results, presented in two-dimensional and three-dimensional formats in Fig. 9B, revealed that the pyridine moiety of **T8** enters the NAM binding region. This interaction was characterized by the formation of multiple hydrogen bonds with adjacent residues Ser275 and Arg311 and a π–π stacking interaction with Tyr188. Similar to its interaction with NQO1, the benzoquinone part of **T8** extended to the solvent area of the NAMPT protein. The docking analyses unveiled a dual mechanism of action for compound **T8**. In NQO1, the benzoquinone moiety of **T8** interacted well within the protein cavity, forming strong hydrogen bonds with key residues. Conversely, in NAMPT, the key pharmacophore of the NAMPT inhibitor in **T8** was effectively bound to the enzyme, forming multiple hydrogen bonds that stabilize the interaction.

Conclusion

In this work, we designed and synthesized a series of compounds that target NQO1 and NAMPT. Our comprehensive *in vitro* evaluations revealed that these compounds, particularly compound **T8**, exhibit promising antitumor efficacy. The antitumor activity of the compounds, especially **T8**, was validated to be NQO1-dependent using MDA-MB-231 (NQO1$^{+/-}$) cell models. Compound **T8** stood out due to its potent antitumor activity, characterized by enhancing intracellular ROS levels *via* NQO1-mediated redox cycling, inhibiting NAMPT activity, increasing NAD^+ consumption, and ultimately inducing cancer cell apoptosis.

In summary, this study has successfully identified compound **T8** as a potential antitumor candidate, with preliminary validations suggesting a promising mechanism of action. Despite its notable *in vitro* antitumor activity, **T8**'s poor water solubility presents a significant limitation in terms of achievable dosage. Future research efforts will focus on structural optimization to enhance solubility. This may include adopting a prodrug strategy or refining the drug delivery system to improve the formulation. Additionally, the current scope of research is primarily confined to cellular and protein-level analyses. Moving forward, the plan is to evaluate the antitumor efficacy of compound **T8** *in vivo* using tumor-bearing mouse models. This next phase will provide deeper insights into the compound's mechanism of action and explore its potential across various cancer types. The over-

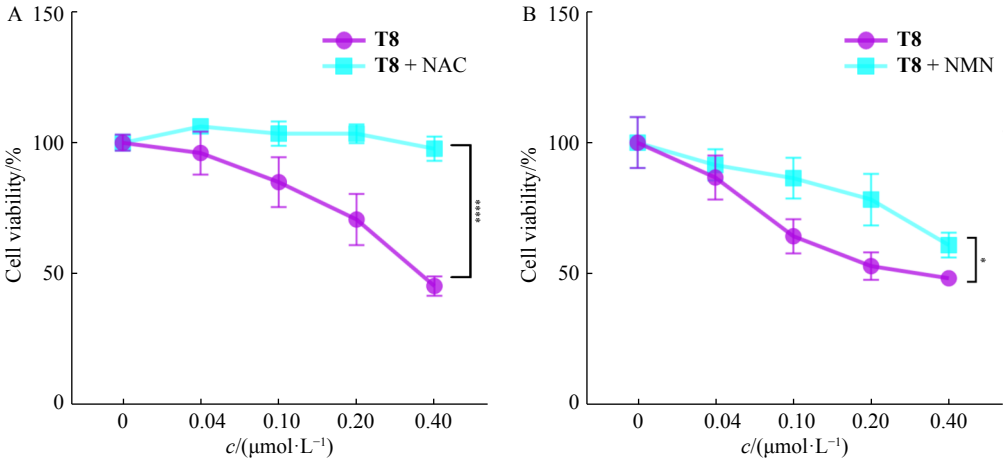

Fig. 6 Cell viability curves of MCF-7 cell growth by different concentrations of compound T8 in the presence or absence of (A) NAC (1 mmol·L^{-1}) and (B) NMN (200 μmol·L^{-1}). MCF-7 cells were individually co-incubated with compound T8 and NAC or NMN for 24 h. Cell viability was tested using the CCK-8 assay. Data are presented as the mean ± SD (n = 6/group). Two-way ANOVA tests were performed. $^{*}P < 0.05$, $^{****}P < 0.0001$ *vs* T8 group.

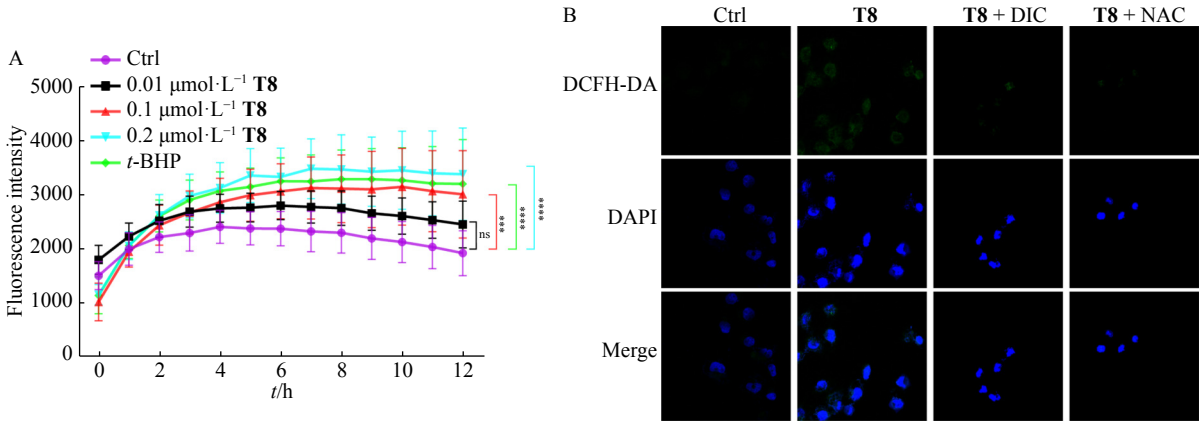

Fig. 7 Measurement of ROS levels in MCF-7 cells. (A) Intracellular ROS was measured using the DCFH-DA probe, with *t*-BHP as a positive control. (B) Colocalization of the fluorescence images of ROS using the DCFH-DA probe. MCF-7 cells were separately cultured with T8 (20 μmol·L^{-1}, 10 h), T8 (20 μmol·L^{-1}, 10 h) + DIC (5 mmol·L^{-1}, 6 h), T8 (20 μmol·L^{-1}, 10 h) + NAC (5 mmol·L^{-1}, 6 h), and negative control. Data are presented as the mean ± SD (n = 6/group). Two-way ANOVA tests were performed. $^{***}P < 0.001$, $^{****}P < 0.0001$ *vs* Control.

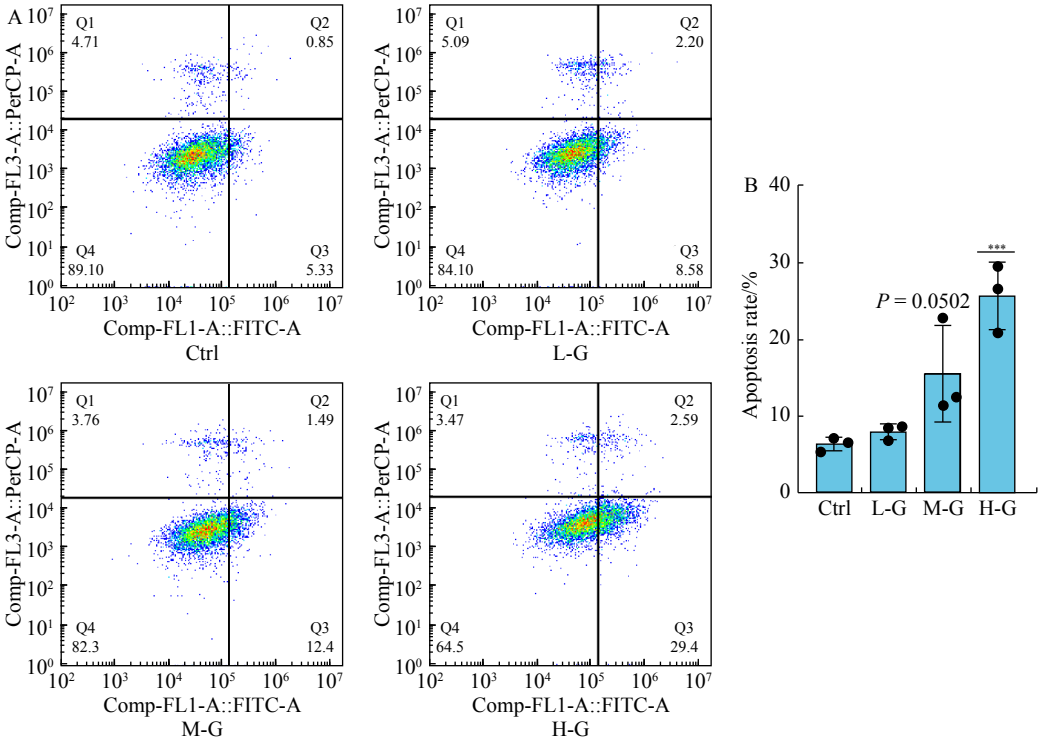

Fig. 8 Compound T8 induced the apoptosis of MCF-7 cells in a dose-dependent manner. (A) Flow cytometry analysis of Annexin V/PI staining of apoptotic MCF-7 cells. MCF-7 cells were treated with the different concentrations (L-G, 0.04 μmol·L^{-1}; M-G, 0.08 μmol·L^{-1}; H-G, 0.1 μmol·L^{-1}) of compound T8 for 24 h using AV/PI staining. (B) Quantitative analysis of apoptotic cells. Data are presented as the mean ± SD (n = 3/group). One-way ANOVA tests were performed. $^{***}P < 0.001$ *vs* Control.

arching goal is to advance our understanding of compound **T8**'s therapeutic potential and to expand its clinical applicability.

Experimental

General chemicals and instruments

All chemicals and solvents were obtained commercially and utilized as received, except where specifically mentioned. ^{1}H NMR and ^{13}C NMR spectra were recorded on a Bruker AVANCE AV300 (300 MHz) or AVANCE AV500 (500 MHz) with tetramethylsilane (TMS) as an internal standard at room temperature. Mass spectrometry (MS) was conducted by an Agilent (USA) Model 1946A-MSD mass spectrometer (ESI-MS), and high-resolution mass spectrometry (HR-MS) was determined by a Waters Q-Time of Flight micro mass spectrometer (USA). The experimental GF254 thin-layer chromatography plate (TLC) was purchased from Qingdao Ocean Chemical Plant, and the preparative TLC was pur-

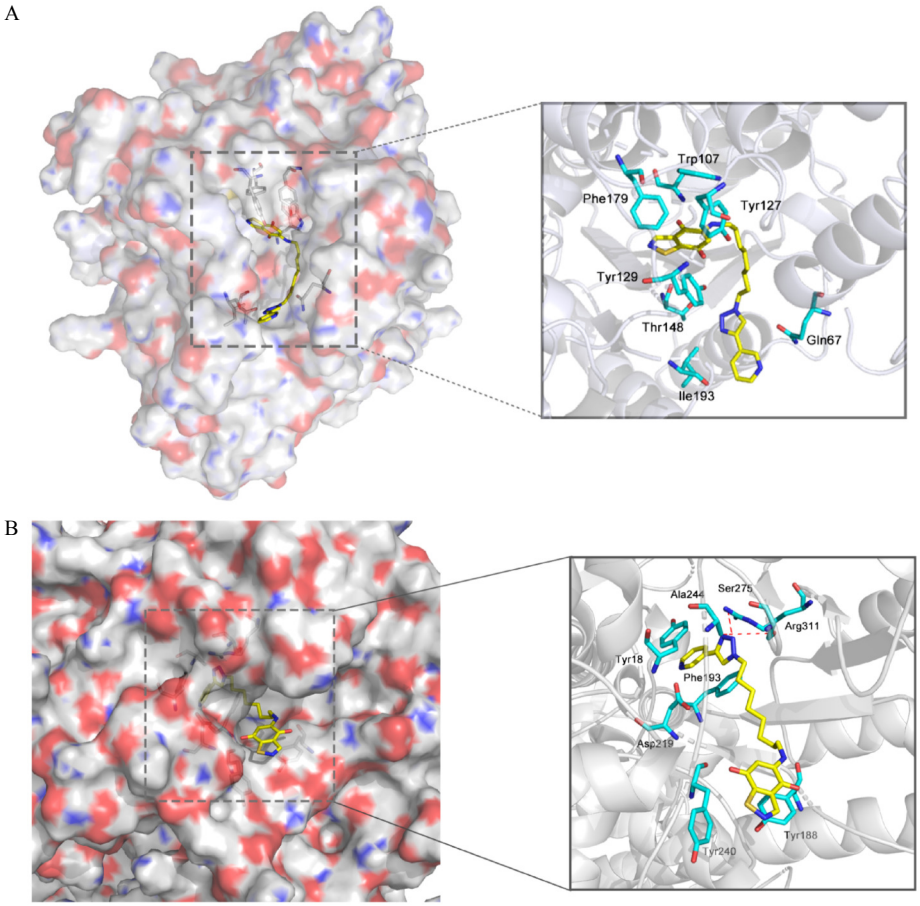

Fig. 9 Binding modes of compound T8 with NQO1 (PDB ID: 2F1O) and NAMPT (PDB ID: 2GVJ). (A) Bind mode of compound T8 to NQO1. (B) Binding mode of compound T8 to NAMPT.

chased from Shandong Dexin Chemical Plant.

Tert-butyl4-(4-hydroxybutyl)piperidine-1-carboxylate(**2**). Compound **1** (1.57 g, 10 mmol, 1 equiv) was dissolved in a 1 : 1 mixture of THF/H_2O (20 mL) and cooled to 0 °C. Boc_2O (2.6 g, 12 mmol, 1.2 equiv) was then added dropwise. The mixture was stirred at room temperature overnight. After the removal of the organic solvent, the mixture was extracted with EtOAc. The organic layers were combined, washed with brine, dried over sodium sulfate, filtered, and concentrated, yielding compound **2** as a transparent oil.

Tert-butyl4-(4-(1,3-dioxoisoindolin-2-yl)butyl)piperidine-1-carboxylate (**3**). A solution of compound **2** (0.77 g, 3 mmol, 1 equiv), phthalimide (0.44 g, 3 mmol, 1 equiv), and PPh_3 (0.94 g, 3.6 mmol, 1.2 equiv) was stirred in dry THF (12 mL) at 0 °C under a nitrogen atmosphere. DEAD (0.63 g, 3.6 mmol, 1.2 equiv) was then added dropwise. The reaction mixture was then allowed to warm to room temperature and stirred for 16 h. Post-reaction, the solvent was removed, and the product was recrystallized from EtOAc and then purified by column chromatography and recrystallization with isopropanol, yielding compound **3** as a white solid.

Tert-butyl 4-(4-aminobutyl)piperidine-1-carboxylate (**4**). Compound **3** (1.16 g, 3 mmol, 1 equiv) was dissolved in EtOH (12 mL), followed by the addition of hydrazine hydrate (0.3 g, 6 mmol, 2 equiv). The mixture was refluxed until completion. After filtration, the solvent was evaporated, yielding compound **4** as a white oil.

Tert-butyl (E)-4-(4-(3-(pyridin-3-yl)acr-ylamido)butyl)piperidine-1-carboxylate (**5**). 3-Pyridineacrylic acid (0.18 g, 1.22 mmol, 1 equiv) was dissolved in CH_2Cl_2 (3 mL), followed by the addition of thionyl chloride (0.3 g, 2.44 mmol, 2 equiv) for 2 h at room temperature. After solvent removal, the resulting product was added to a CH_2Cl_2 (5 mL) and DIEA (0.19 g, 1.46 mmol, 1.2 equiv) solution of compound **4** at room temperature. The mixture was stirred overnight at the same temperature. The mixture was washed with brine, dried over sodium sulfate, and filtered, and the solvent was removed. The residue was purified by column chromatography, yielding compound **5** as a white solid.

(E)-N-(4-(piperidin-4-yl)butyl)-3-(pyrid-in-3-yl)acrylamide (**6**). Hydrochloric acid 2 mol·L^{-1} (2.64 mmol, 1.32 mL, 2 equiv) in ethanol was added dropwise to compound **5** (0.51 g, 1.32 mmol, 1 equiv) overnight at 0 °C. The solvent was then removed, yielding compound **6** as a yellow solid.

(E)-N-(4-(1-(4,7-dioxo-4,7-dihydroben-zo[d]isothiazol-5-yl)piperidin-4-yl)buty-l)-3-(pyridin-3-yl)acrylamide (**P2**). The compound **6** (1.32 mmol, 0.38 g, 1.1 equiv) was dissolved in CH_2Cl_2 (4 mL), followed by the addition of DIEA (3.6 mmol,

0.47 g, 3 equiv) and cerium trichloride (0.12 mmol, 0.03 g, 0.1 equiv), and then 1,2-benzisothiazole-4,7-dione (1.2 mmol, 0.19 g, 1 equiv) was added for 5 h at room temperature. Upon completion, water was added, and the product was extracted with CH_2Cl_2. The crude product was purified by column chromatography (DCM : *i*-PrOH, 150 : 1) to yield compound **P2** as a purple-black solid: yield 65%; ^{1}H NMR (300 MHz, DMSO-d_6) δ: 8.96 (s, 1H), 8.73 (s, 1H), 8.53 (d, J = 4.5 Hz, 1H), 8.12 (s, 2H), 7.95 (d, J = 7.7 Hz, 1H), 7.45−7.40 (m, 2H), 6.71 (d, J = 15.9 Hz, 1H), 5.88 (s, 1H), 3.18−3.02 (m, 4H), 1.76 (d, J = 12.0 Hz, 2H), 1.57−1.43 (m, 4H), 1.32−1.22 (m, 6H). ^{13}C NMR (75 MHz, DMSO-d_6) δ: 156.69, 149.92, 148.91, 134.95, 133.79, 124.27, 123.83, 105.99, 49.71, 35.23, 34.64, 31.74; ESI-HR-MS: calculated for [M + H]$^+$ 451.1798, found 451.1811.

*General procedures for the preparation of **8a**−**8f***. The corresponding diamines **7a**−**7f** (1 equiv) were dissolved in THF/H_2O (1 : 1). At 0 °C, Boc_2O (0.3 equiv) was added dropwise, and then the reaction mixture returned to room temperature overnight. The organic solvent was removed, and then the reaction mixture was extracted with EtOAc. The organic layers were combined, washed with brine, dried over sodium sulfate, filtered, and concentrated to yield compounds **8a**−**8f** as colorless oils, which were used in the next step without further purification.

*General procedures for the preparation of **9a**−**9f***. 3-Pyridineacrylic acid (1 equiv) was dissolved in CH_2Cl_2 (0.3 mol·L^{-1}), followed by the addition of thionyl chloride (3 equiv) for 2 h at room temperature. After removing the solvent, this compound was slowly added to the mixture of CH_2Cl_2 (0.3 mol·L^{-1}) and DIEA (1.5 equiv) of corresponding **8a**−**8f** (1 equiv) at room temperature. The mixture was stirred overnight at room temperature, washed with brine, dried over sodium sulfate, filtered, and concentrated. The residue was purified by column chromatography.

*General procedures for the preparation of **10a**−**10f***. Hydrochloric acid 2 mol·L^{-1} (2 equiv) in ethanol was added dropwise to corresponding **9a**−**9f** (1 equiv) and stirred overnight at 0 °C. The solvent was removed to yield compound **10a**−**10f** as white solids.

*General procedures for the preparation of **P3**−**P8***. The corresponding amine **10a**−**10f** (1.1 equiv) was dissolved in CH_2Cl_2 (0.3 mol·L^{-1}), followed by the addition of DIEA (3 equiv) and cerium trichloride (0.1 equiv), and then 1,2-benzisothiazole-4,7-dione (1 equiv) was added for 5 h at room temperature. After completion of the reaction, water was added, and the desired product was extracted with CH_2Cl_2. Finally, the crude product was purified by column chromatography (DCM : *i*-PrOH, 150 : 1), yielding compounds **P3**−**P8** as purple-black solids.

(E)-N-(3-((4,7-dioxo-4,7-dihydrobenzo-[d]isothiazol-5-yl)amino)propyl)-3-(pyridin-3-yl)acrylamide (**P3**). ^{1}H NMR (300 MHz, DMSO-d_6) δ: 9.02 (s, 1H), 8.75 (s, 1H), 8.54 (d, J = 3.8 Hz, 1H), 8.23 (m, 1H), 8.02−7.96 (m, 2H), 7.48−7.41 (m, 2H), 6.71 (d, J = 15.9 Hz, 1H), 5.62 (s, 1H), 3.33−3.24 (m, 4H), 1.81−1.76 (m, 2H); ^{13}C NMR (75 MHz, DMSO-d_6) δ: 175.81, 175.33, 164.68, 156.33, 150.17, 150.05, 149.04, 135.29, 133.89, 130.66, 124.09, 123.91, 97.08, 36.42, 27.25; ESI-HR-MS: calculated for [M + H]$^+$ 369.1016, found 369.1027.

(E)-N-(4-((4,7-dioxo-4,7-dihydrobenzo-[d]isothiazol-5-yl)amino)butyl)-3-(pyridin-3-yl)acrylamide (**P4**). ^{1}H NMR (300 MHz, DMSO-d_6) δ: 9.01 (s, 1H), 8.72 (s, 1H), 8.52 (d, J = 4.0 Hz, 1H), 8.15 (m, 1H), 8.03 (s, 1H), 7.93 (d, J = 7.7 Hz, 1H), 7.44−7.39 (m, 2H), 6.69 (d, J = 15.9 Hz, 1H), 5.60 (s, 1H), 3.29−3.19 (m, 4H), 1.60−1.50 (m, 4H); ^{13}C NMR (75 MHz, DMSO-d_6) δ: 175.83, 175.20, 167.63, 164.58, 156.31, 151.59, 150.17, 148.24, 134.76, 133.73, 123.30, 96.87, 42.49, 28.86, 27.11, 26.10; ESI-HR-MS: calculated for [M + H]$^+$ 383.1172, found 383.1176.

(E)-N-(5-((4,7-dioxo-4,7-dihydrobenzo-[d]isothiazol-5-yl)amino)pentyl)-3-(pyridin-3-yl)acrylamide (**P5**). ^{1}H NMR (300 MHz, DMSO-d_6) δ: 9.02 (s, 1H), 8.73 (s, 1H), 8.54 (d, J = 3.8 Hz, 1H), 8.13 (m, 1H), 8.02 (m, 1H), 7.95 (d, J = 7.9Hz, 1H), 7.45−7.37 (m, 2H), 6.71 (d, J = 15.9 Hz, 1H), 5.59 (s, 1H), 3.22−3.17 (m, 4H), 1.63−1.59 (m, 2H), 1.50−1.47 (m, 2H), 1.34−1.30 (m, 2H); ^{13}C NMR (75 MHz, DMSO-d_6) δ: 175.84, 175.20, 174.36, 167.63, 164.22, 156.27, 150.15, 148.61, 147.69, 135.22, 134.48, 133.71, 131.32, 124.95, 124.40, 96.94, 42.48, 38.52, 33.61, 29.78, 26.84; ESI-HR-MS: calculated for [M + H]$^+$ 397.1329, found 397.1340.

(E)-N-(6-((4,7-dioxo-4,7-dihydrobenzo-[d]isothiazol-5-yl)amino)hexyl)-3-(pyridin-3-yl)acrylamide (**P6**). ^{1}H NMR (300 MHz, DMSO-d_6) δ: 9.01 (s, 1H), 8.72 (s, 1H), 8.52 (d, J = 4.0 Hz, 1H), 8.16 (m, 1H), 8.01 (m, 1H), 7.94 (d, J = 7.9 Hz, 1H), 7.44−7.38 (m, 2H), 6.69 (d, J = 15.9 Hz, 1H), 5.56 (s, 1H), 3.20-3.15 (m, 4H), 1.57 (m, 2H), 1.45 (m, 2H), 1.32 (m, 4H); ^{13}C NMR (75 MHz, DMSO-d_6) δ: 157.25, 156.26, 150.13, 149.91, 134.93, 133.77, 124.27, 123.82, 96.83, 42.45, 38.54, 28.89, 27.06, 26.03; ESI-HR-MS: calculated for [M + H]$^+$ 411.1485, found 411.1501.

(E)-N-(7-((4,7-dioxo-4,7-dihydrobenzo-[d]isothiazol-5-yl)amino)heptyl)-3-(pyridin-3-yl)acrylamide (**P7**). ^{1}H NMR (300 MHz, DMSO-d_6) δ: 9.02 (s, 1H), 8.73 (s, 1H), 8.53 (d, J = 3.9 Hz, 1H), 8.13 (m, 1H), 8.02 (m, 1H), 7.95 (d, J = 7.9 Hz, 1H), 7.45−7.40 (m, 2H), 6.71 (d, J = 15.9 Hz, 1H), 5.57 (s, 1H), 3.19−3.16 (m, 4H), 1.58 (m, 2H), 1.46 (m, 2H), 1.31−1.23 (m, 6H); ^{13}C NMR (75 MHz, DMSO-d_6) δ: 176.37, 175.77, 164.91, 156.87, 150.71, 150.53, 149.51, 135.62, 134.34, 131.18, 124.70, 97.48, 42.71, 38.78, 27.05, 25.19; ESI-HR-MS: calculated for [M + H]$^+$ 425.1642, found 425.1653.

(E)-N-(8-((4,7-dioxo-4,7-dihydrobenzo-[d]isothiazol-5-yl)amino)octyl)-3-(pyridin-3-yl)acrylamide (**P8**). ^{1}H NMR (300 MHz, DMSO-d_6) δ: 9.03 (s, 1H), 8.74 (s, 1H), 8.54 (d, J = 3.7 Hz, 1H), 8.12 (m, 1H), 8.01−7.95 (m, 2H), 7.46−7.41 (m, 2H), 6.71 (d, J = 15.9 Hz, 1H), 5.57 (s, 1H), 3.18−3.13 (m, 4H), 1.58 (m, 2H), 1.45 (m, 2H), 1.29 (m, 8H); ^{13}C NMR (75 MHz, DMSO-d_6) δ: 156.31, 149.96, 148.95, 134.97,

133.83, 130.71, 124.34, 123.88, 96.86, 42.53, 29.00, 28.58, 27.14, 26.34; ESI-HR-MS: calculated for $[M + H]^+$ 439.1798, found 439.1802.

General procedures for the preparation of ***12a*****−*****12d***. The corresponding commercially available bromo derivatives (**11a**−**11d**) (1 equiv) were dissolved in DMF (0.4 mol·L^{-1}). Sodium azide was added (1.2 equiv) while stirring at room temperature, and the reaction mixture was heated at 80 °C overnight. After completion of the reaction, water was added, and the desired product was extracted with EtOAc. The organic layers were combined, washed with water and brine, dried over sodium sulfate, and concentrated under vacuum to yield the desired azides, which were used in the subsequent step without further purification.

General procedures for the preparation of ***13a*****−*****13d***. 3-Ethynylpyridine (1 equiv) and the corresponding azide (**12a**−**12d**) (1 equiv) were suspended in a mixture of water/tert-butanol (1 ∶ 1), and sodium ascorbate (0.1 equiv), a freshly prepared 1 mol·L^{-1} solution in water, was added, followed by the addition of copper(II) sulfate pentahydrate (0.01 equiv). The resulting mixture was heated to 40 °C and stirred for 12 h. After completion of the reaction, water was added, and the desired product was extracted with EtOAc. Finally, the crude product was purified by column chromatography, yielding the desired triazoles.

General procedures for the preparation of ***14a*****−*****14d***. Under a nitrogen atmosphere, DPPA (diphenylphosphoryl azide, 2 equiv) and 1,8-diazabicyclo[5.4.0]undec-7-ene (DBU) (2 equiv) were added to a cooled (0 °C) solution of the corresponding alcohol (**14a**−**14d**) (1 equiv) in DMF (0.4 mol·L^{-1}). After 30 min, NaN_3 (2 equiv) was added, and the reaction mixture was heated at 100 °C for 3 h. The reaction mixture was then cooled to room temperature, diluted with water, and extracted with EtOAc. The combined organic layers were washed with water and brine, dried over sodium sulfate, and concentrated *in vacuo*. Finally, the crude product was purified by column chromatography.

General procedures for the preparation of ***15a*****−*****15d***. Water (6 equiv) and triphenyl-phosphine (1.5 equiv) were added to a solution of the corresponding azide (**14a**−**14d**) (1 equiv) in THF (0.3 mol·L^{-1}). The resulting mixture was heated at reflux for 3 h under magnetic stirring. The solvent was evaporated *in vacuo*, and the residue was purified by column chromatography.

General procedures for the preparation of ***T5*****−*****T8***. The corresponding amine **15a**−**15d** (1.1 equiv) was dissolved in CH_2Cl_2 (0.3 mol·L^{-1}), followed by the addition of DIEA (3 equiv) and cerium trichloride (0.1 equiv), and then 1,2-benzisothiazole-4,7-dione (1 equiv) was added for 5 h at room temperature. After completion of the reaction, water was added, and the desired product was extracted with CH_2Cl_2. Finally, the crude product was purified by column chromatography (DCM ∶ *i*-PrOH, 150 ∶ 1), yielding compounds **T5**−**T8** as purple-black solids.

5-((5-(4-(pyridin-3-yl)-1H-1,2,3-triazol-1-yl)pentyl)amino) benzo[d]isothiazole-4,7-dione (**T5**). ^{1}H NMR (300 MHz, DMSO-d_6) δ: 9.03 (s, 1H), 9.00 (s, 1H), 8.70 (s, 1H), 8.55−8.53 (m, 1H), 8.22−8.19 (m, 1H), 8.01−7.98 (m, 1H), 7.59 (dd, J = 7.86, 4.86 Hz, 1H), 5.57 (s, 1H), 4.43 (t, J = 6.69 Hz, 2H), 3.24−3.17 (m, 2H), 1.96−1.87 (m, 2H), 1.68−1.59 (m, 2H), 1.37−1.30 (m, 2H); ^{13}C NMR (75 MHz, DMSO-d_6) δ: 178.89, 178.31, 170.67, 159.34, 153.20, 151.45, 149.01, 146.40, 136.78, 135.72, 129.99, 127.15, 125.03, 100.11, 52.58, 45.33, 32.21, 29.60, 26.35; ESI-HR-MS: calculated for $[M + H]^+$ 395.1285, found 395.1292.

5-((6-(4-(pyridin-3-yl)-1H-1,2,3-triazol-1-yl)hexyl)amino)benzo[d]isothiazole-4,7-dione (**T6**). ^{1}H NMR (300 MHz, DMSO-d_6) δ: 9.03 (d, J = 1.5 Hz, 1H), 9.02 (s, 1H), 8.70 (s, 1H), 8.53 (dd, J = 4.71, 1.38 Hz, 1H), 8.21−8.18 (m, 1H), 8.02−7.98 (m, 1H), 7.47 (dd, J = 7.83, 4.83 Hz, 1H), 5.57 (s, 1H), 4.44−4.30 (m, 2H), 3.23−3.18 (m, 2H), 1.91−1.86 (m, 2H), 1.61−1.56 (m, 2H), 1.34 (m, 4H); ^{13}C NMR (75 MHz, DMSO-d_6) δ: 178.92, 178.31, 159.39, 153.25, 151.82, 149.39, 146.53, 136.78, 135.36, 129.85, 127.00, 124.94, 100.01, 52.63, 45.53, 32.51, 30.04, 28.85, 28.58; ESI-HR-MS: calculated for $[M + H]^+$ 409.1441, found 409.1456.

5-((7-(4-(pyridin-3-yl)-1H-1,2,3-triazol-1-yl)heptyl)amino) benzo[d]isothiazole-4,7-dione (**T7**). ^{1}H NMR (300 MHz, DMSO-d_6) δ: 9.04 (m, 1H), 9.02 (s, 1H), 8.70 (s, 1H), 8.53−8.52 (m, 1H), 8.21−8.18 (m, 1H), 8.03−7.99 (m, 1H), 7.47 (dd, J = 7.86, 4.86 Hz, 1H), 5.56 (s, 1H), 4.42 (t, J = 7.02 Hz, 2H), 3.22−3.15 (m, 2H), 1.89−1.85 (m, 2H), 1.56−1.54 (m, 2H), 1.31 (m, 6H); ^{13}C NMR (75 MHz, DMSO-d_6) δ: 178.92, 178.28, 159.38, 153.23, 151.81, 149.39, 136.81, 135.34, 129.85, 126.99, 124.93, 99.98, 52.65, 45.58, 32.54, 32.04, 31.07, 30.16, 29.28, 28.80; ESI-HR-MS: calculated for $[M + H]^+$ 423.1598, found 423.1610.

5-((8-(4-(pyridin-3-yl)-1H-1,2,3-triazol-1-yl)octyl)amino) benzo[d]isothiazole-4,7-dione (**T8**). ^{1}H NMR (300 MHz, DMSO-d_6) δ: 9.04 (d, J = 1.32 Hz, 1H), 9.03 (s, 1H), 8.72 (s, 1H), 8.54−8.53 (m, 1H), 8.22−8.19 (m, 1H), 8.04 (m, 1H), 7.48 (dd, J = 7.59, 4.92 Hz, 1H), 5.56 (s, 1H), 4.24 (t, J = 6.99 Hz, 2H), 3.20−3.17 (m, 2H), 1.87 (m, 2H), 1.56 (m, 2H), 1.29 (m, 8H); ^{13}C NMR (75 MHz, DMSO-d_6) δ: 176.33, 175.70, 156.85, 150.66, 149.21, 146.75, 143.91, 134.23, 132.80, 127.27, 124.46, 122.38, 97.34, 50.08, 43.00, 30.00, 28.95, 28.77, 27.62, 26.80, 26.24; ESI-HR-MS: calculated for $[M + H]^+$ 437.1754, found 437.1770.

Cell culture

Human NSLCS cell line (A549), human breast cancer cell lines (MCF-7 and MDA-MB-231), normal mouse hepatocytes (AML-12), and human normal hepatic cell line (L02) were obtained in Shanghai Cell Bank of Chinese Academy of Sciences (Shanghai, China). A549 and MCF-7 cells were cultured in Roswell Park Memorial Institute medium (RPMI) 1640 (Gibco, USA), and L02 and MDA-MB-231 cells were cultured in Dulbecco's modified Eagle's medium (DMEM, Gibco, USA) supplemented with 10% fetal bovine serum (FBS, Prime, FSP500, ExCell Bio, China) and 1% penicillin/streptomycin (Gibco, USA). AML-12 cells were

cultured in Dulbecco's modified Eagle's medium: F-12 (DMEM/F12, Gibco, USA) supplemented with 10% fetal bovine serum (FBS, Prime, FSP500, ExCell Bio, China), 1% penicillin/streptomycin (Gibco, USA), dexamethasone 40 ng·mL^{-1} (Sigma, USA), and 1% insulin (ITS-G, Gibco, USA). All cell lines were maintained at 37 °C in a humidified atmosphere with 5% CO_2 and 95% air. Subculturing was performed every 2−3 days.

Cell viability assay

Cells in the logarithmic growth phase were seeded into 96-well plates (5000−8000 cells/well). After overnight incubation, the medium containing the compounds was added, and the cells were cultured for an additional 24 h. The cells were then fixed with 10% trichloroacetic acid at 4 °C, washed with water, and air-dried. Subsequently, the cells were stained with 0.057% SRB solution, washed with 1% acetic acid, and dissolved in 10 mmol·L^{-1} Tris solution. Finally, the optical density at the wavelength of 510 nm (OD_{510}) was measured.

Western blotting analysis

Total proteins were extracted from cultured cells using ice-cold RIPA lysis containing 1% protease inhibitor cocktail. Cytoplasmic and nuclear proteins were isolated using the Nuclear and Cytoplasmic Protein Extraction Kit (Beyotime Institute of Biotechnology, Jiangsu, China) following the manufacturer's protocol. Protein concentration was measured by BCA assay (Vazyme, China). Proteins (40 μg/lane) were separated by SDS-PAGE on 10% or 12% polyacrylamide gels and transferred to PVDF membranes *via* electroblotting. Membranes were blocked in 5% non-fat dry milk in tris-buffered saline with 0.1% Tween 20 at 37 °C for 1 h, followed by overnight incubation with primary antibodies at 4 °C and then 1 h with secondary antibodies at 37 °C. Blots were developed using an enhanced chemiluminescence kit (Thermo Fisher Scientific, Waltham, MA). The signals were captured using a ChemiDoc XRS$^+$ system (Bio-Rad Laboratories, Hercules, CA). Antibodies against NAMPT (#86634, D7V5J), NQO1 (#62262, D6H3A), and GAPDH (#5174, D16H11) were purchased from Cell Signal Technology.

In vitro NQO1 assay

Human NQO1 protein (MCE, USA), compound **T8**, and PBS solution were added to each well of a 96-well plate, making up a total volume of 196 μL. Subsequently, 4 μL of NAD(P)H (20 mmol·L^{-1}) was added. The OD_{340} value was immediately measured and continuously read every 2 s for a total of 5 min.

In vitro NAMPT assay

The inhibitory activity of NAMPT was determined using the CycLex NAMPT colorimetric assay kit (CycLex NAMPT colorimetric assay kit Ver.2, MBL International Corp., Woburn, MA) according to the manufacturer's protocol.

Construction of NQO1 overexpressing cell line

MDA-MB-231 (NQO1-) cells were cultured to reach the logarithmic growth phase. The cells were then resuspended in DMEM supplemented with 10% fetal bovine serum and 1% penicillin/streptomycin (20 000 cells·mL^{-1}). The resuspended cells were seeded into 6-well plates and incubated for 24 h. The medium in the 6-well plates was replaced. Polybrene (5 μg·mL^{-1}) was added to each well, and the appropriate number of virus-infected cells were added for 8−12 h [virus volume = (MOI × cell number)/viral titer]. The cells were continuously cultured post-infection. Western blotting analysis was subsequently performed to verify the successful construction of NQO1 overexpressing cells.

Measurement of cellular NAD$^+$ content

Cellular NAD$^+$ levels were quantified using the NAD$^+$ test kit (WST-8, Beyotime Biotechnology, Nanjing, China) according to the manufacturer's protocols.

Measurement of cellular ROS levels

Cellular ROS levels were determined using a DCFH-DA probe (MCE, USA). MCF-7 cells (15 000 cells/well) were seeded into 96-well plates for 24 h. After discarding the medium, cells were stained with a DCFH-DA probe (10 μmol·L^{-1}) for 30 min, followed by washing with PBS twice. Later, different concentrations of compound **T8** were added. MCF-7 cells were treated with *t*-BHP (100 μmol·L^{-1}) as a positive control. Finally, fluorescence intensity was measured at an excitation wavelength of 488 nm and an emission wavelength of 525 nm. For colocalization studies, MCF-7 cells were treated with compound **T8** (20 μmol·L^{-1}, 10 h), **T8** (20 μmol·L^{-1}, 10 h) + DIC (5 mmol·L^{-1}, 6 h), **T8** (20 μmol·L^{-1}, 10 h) + NAC (5 mmol·L^{-1}, 6 h), and the negative control. Post-treatment, the cells were incubated with the DCFH-DA probe (10 μmol·L^{-1}) for 30 min. After the cell culture medium was discarded, the MCF-7 cells were washed once and fixed with 4% paraformaldehyde (Beyotime, China) for 10 min. After three washes with PBS, the cells were stained with DAPI dye (1 ∶ 5000, PBS dilution, Sigma, USA) for 10 min and washed again with PBS twice. The fluorescence was observed under a laser scanning confocal microscope (Zeiss LSM700, Germany). All experimental procedures were conducted under light-protected conditions.

In vitro cell selectivity assay

Cells in the logarithmic growth phase were seeded into 96-well plates (10 000−15 000 cells/well), with a total volume of 100 μL per well. After 24 h of culture, an FBS-free medium containing varying concentrations of compound **T8** was added, and then the cells were further cultured for 24 h. To each well, 10 μL of CCK-8 solution was added, and the plates were incubated at 37 °C for 1−4 h to measure OD_{450}. All experimental procedures were conducted under light-protected conditions.

Apoptosis analysis by flow cytometry

MCF-7 cells were treated with different concentrations (L-G, 0.04 μmol·L^{-1}; M-G, 0.08 μmol·L^{-1}; H-G, 0.1 μmol·L^{-1}) of compound **T8** for 24 h. Post-treatment, in accordance with the AV/PI staining protocol (BD, USA), the fluorescence intensity was analyzed using a flow cytometer (BD, AccuriTM C6 Plus, USA).

Molecular docking

The crystal structures of the proteins NQO1 and NAMPT were obtained from the Protein Databank database, and the PDB IDs were 2F1O and 2GVJ, respectively. Using GOLD 5.1 software, polar hydrogen atoms were added to the crystal structures. Original ligand molecules and water molecules were removed, and energy optimization was performed using the MMFF94 force field. The structures of small molecules for docking were prepared using ChemDraw software. The optimal docking conformations were selected based on scoring and hydrogen bond formation for subsequent analysis.

Statistical analysis

GraphPad Prism 8.0.2 was used for statistical analysis and calculation of various data. All data were presented as mean ± standard deviation (SD). $P < 0.05$ was considered statistically significant. One-way and Two-way ANOVA tests were performed. Significance levels were denoted as $^{*}P < 0.05$, $^{**}P < 0.01$, $^{***}P < 0.001$, and $^{****}P < 0.0001$.

Supplemental Material

Supplemental materials for this paper can be requested by sending E-mails to the corresponding authors.

References

[1] Hanahan D, Weinberg RA. The hallmarks of cancer [J]. *Cell*, 2000, **100**(1): 57-70.

[2] Hanahan D, Weinberg RA. Hallmarks of cancer: the next generation [J]. *Cell*, 2011, **144**(5): 646-674.

[3] Yaku K, Okabe K, Hikosaka K, *et al*. NAD metabolism in cancer therapeutics [J]. *Front Oncol*, 2018, **8**: 622.

[4] Kennedy BE, Sharif T, Martell E, *et al*. NAD^+ salvage pathway in cancer metabolism and therapy [J]. *Pharmacol Res*, 2016, **114**: 274-283.

[5] Belenky P, Bogan KL, Brenner C. NAD^+ metabolism in health and disease [J]. *Trends Biochem Sci*, 2007, **32**(1): 12-19.

[6] Luengo A, Gui DY, Vander HMG. Targeting metabolism for cancer therapy [J]. *Cell Chem Biol*, 2017, **24**(9): 1161-1180.

[7] Pink JJ, Planchon SM, Tagliarino C, *et al*. NAD(P)H: quinone oxidoreductase activity is the principal determinant of beta-lapachone cytotoxicity [J]. *J Biol Chem*, 2000, **275**(8): 5416-5424.

[8] Zhu H, Li YB. NAD(P)H: quinone oxidoreductase 1 and its potential protective role in cardiovascular diseases and related conditions [J]. *Cardiovasc Toxicol*, 2012, **12**(1): 39-45.

[9] Siegel D, Yan C, Ross D. NAD(P)H: quinone oxidoreductase 1 (NQO1) in the sensitivity and resistance to antitumor quinones [J]. *Biochem Pharmacol*, 2012, **83**(8): 1033-1040.

[10] Winski SL, Koutalos Y, Bentley DL, *et al*. Subcellular localization of NAD(P)H: quinone oxidoreductase 1 in human cancer cells [J]. *Cancer Res*, 2002, **62**(5): 1420-1424.

[11] Nakamura M, Hayashi T. One- and two-electron reduction of quinones by rat liver subcellular fractions [J]. *J Biochem*, 1994, **115**(6): 1141-1147.

[12] Park EJ, Min KJ, Lee TJ, *et al*. *β*-Lapachone induces programmed necrosis through the RIP1-PARP-AIF-dependent pathway in human hepatocellular carcinoma SK-Hep1 cells [J]. *Cell Death Dis*, 2014, **5**(5): e1230.

[13] Ross D, Kepa JK, Winski SL, *et al*. NAD(P)H: quinone oxidoreductase 1 (NQO1): chemoprotection, bioactivation, gene regulation and genetic polymorphisms [J]. *Chem Biol Interact*, 2000, **129**(1-2): 77-97.

[14] Chakrabarti G, Silvers MA, Ilcheva M, *et al*. Tumor-selective use of DNA base excision repair inhibition in pancreatic cancer using the NQO1 bioactivatable drug, *β*-lapachone [J]. *Sci Rep*, 2015, **5**: 17066.

[15] Moore Z, Chakrabarti G, Luo X, *et al*. NAMPT inhibition sensitizes pancreatic adenocarcinoma cells to tumor-selective, PAR-independent metabolic catastrophe and cell death induced by *β*-lapachone [J]. *Cell Death Dis*, 2015, **6**(1): e1599.

[16] Wang GY, Zhang L, Geng YD, *et al*. *β*-Elemene induces apoptosis and autophagy in colorectal cancer cells through regulating the ROS/AMPK/mTOR pathway [J]. *Chin J Nat Med*, 2022, **20**(1): 9-21.

[17] Dong Y, Bey EA, Li LS, *et al*. Prostate cancer radiosensitization through poly(ADP-Ribose) polymerase-1 hyperactivation [J]. *Cancer Res*, 2010, **70**(20): 8088-8096.

[18] Bey EA, Bentle MS, Reinicke KE, *et al*. An NQO1- and PARP-1-mediated cell death pathway induced in non-small-cell lung cancer cells by beta-lapachone [J]. *Proc Natl Acad Sci USA*, 2007, **104**(28): 11832-11837.

[19] Cresteil T, Jaiswal AK. High levels of expression of the NAD(P)H: quinone oxidoreductase (NQO1) gene in tumor cells compared to normal cells of the same origin [J]. *Biochem Pharmacol*, 1991, **42**(5): 1021-1027.

[20] Siegel D, Franklin WA, Ross D. Immunohistochemical detection of NAD(P)H: quinone oxidoreductase in human lung and lung tumors [J]. *Clin Cancer Res*, 1998, **4**(9): 2065-2070.

[21] Beall HD, Murphy AM, Siegel D, *et al*. Nicotinamide adenine dinucleotide (phosphate): quinone oxidoreductase (DT-diaphorase) as a target for bioreductive antitumor quinones: quinone cytotoxicity and selectivity in human lung and breast cancer cell lines [J]. *Mol Pharmacol*, 1995, **48**(3): 499-504.

[22] Huang X, Dong Y, Bey EA, *et al*. An NQO1 substrate with potent antitumor activity that selectively kills by PARP1-induced programmed necrosis [J]. *Cancer Res*, 2012, **72**(12): 3038-3047.

[23] Nakae K, Adachi H, Sawa R, *et al*. NAD(P)H quinone oxidoreductase 1 (NQO1)-bioactivated pronqodine A regulates prostaglandin release from human synovial sarcoma cells [J]. *J Nat Prod*, 2013, **76**(4): 510-515.

[24] Mori V, Amici A, Mazzola F, *et al*. Metabolic profiling of alternative NAD biosynthetic routes in mouse tissues [J]. *PLoS One*, 2014, **9**(11): e113939.

[25] Revollo JR, Grimm AA, Imai S. The NAD biosynthesis pathway mediated by nicotinamide phosphoribosyltransferase regulates Sir2 activity in mammalian cells [J]. *J Biol Chem*, 2004, **279**(49): 50754-50763.

[26] Liu HY, Li QR, Cheng XF, *et al*. NAMPT inhibition synergizes with NQO1-targeting agents in inducing apoptotic cell death in non-small cell lung cancer cells [J]. *Chin J Nat Med*, 2016, **14**(8): 582-589.

[27] Zhang KJ, Wang KZ, Zhang XY, *et al*. Discovery of small molecules simultaneously targeting NAD(P)H: quinone oxidoreductase 1 and nicotinamide phosphoribosyltransferase: treatment of drug-resistant non-small-cell lung cancer [J]. *J Med Chem*, 2022, **65**(11): 7746-7769.

[28] Hasmann M, Schemainda I. FK866, a highly specific noncompetitive inhibitor of nicotinamide phosphoribosyltransferase, represents a novel mechanism for induction of tumor cell apoptosis [J]. *Cancer Res*, 2003, **63**(21): 7436-7442.

[29] Holen K, Saltz LB, Hollywood E, *et al*. The pharmacokinetics, toxicities, and biologic effects of FK866, a nicotinamide adenine dinucleotide biosynthesis inhibitor [J]. *Invest New Drugs*, 2008, **26**(1): 45-51.

[30] Galli U, Ercolano E, Carraro L, *et al*. Synthesis and biological evaluation of isosteric analogues of FK866, an inhibitor of

NAD salvage [J]. *Chem Med Chem*, 2008, **3**(5): 771-779.
[31] Colombano G, Travelli C, Galli U, *et al*. A novel potent nicotinamide phosphoribosyltransferase inhibitor synthesized *via* click chemistry [J]. *J Med Chem*, 2010, **53**(2): 616-623.
[32] Olesen UH, Christensen MK, Björkling F, *et al*. Anticancer agent CHS-828 inhibits cellular synthesis of NAD [J]. *Biochem Biophys Res Commun*, 2008, **367**(4): 799-804.
[33] Watson M, Roulston A, Bélec L, *et al*. The small molecule GMX1778 is a potent inhibitor of NAD^+ biosynthesis: strategy for enhanced therapy in nicotinic acid phosphoribosyltransferase 1-deficient tumors [J]. *Mol Cell Biol*, 2009, **29**(21): 5872-5888.
[34] Ravaud A, Cerny T, Terret C, *et al*. Phase I study and pharmacokinetic of CHS-828, a guanidino-containing compound, administered orally as a single dose every 3 weeks in solid tumours: an ECSG/EORTC study [J]. *Eur J Cancer*, 2005, **41**(5): 702-707.
[35] von Heideman A, Berglund A, Larsson R, *et al*. Safety and efficacy of NAD depleting cancer drugs: results of a phase I clinical trial of CHS 828 and overview of published data [J]. *Cancer Chemother Pharmacol*, 2010, **65**(6): 1165-1172.
[36] Blunt CE, Torcuk C, Liu Y, *et al*. Synthesis and intracellular redox cycling of natural quinones and their analogues and identification of indoleamine-2, 3-dioxygenase (IDO) as potential target for anticancer activity [J]. *Angew Chem Int Ed*, 2015, **54**(30): 8740-8745.
[37] Vichai V, Kirtikara K. Sulforhodamine B colorimetric assay for cytotoxicity screening [J]. *Nat Protoc*, 2006, **1**(3): 1112-1116.
[38] Liu P, Li H, Cepeda J, *et al*. Regulation of inflammatory cytokine expression in pulmonary epithelial cells by pre-B-cell colony-enhancing factor *via* a nonenzymatic and AP-1-dependent mechanism [J]. *J Biol Chem*, 2009, **284**(40): 27344-27351.
[39] Skelly JV, Sanderson MR, Suter DA, *et al*. Crystal structure of human DT-diaphorase: a model for interaction with the cytotoxic prodrug 5-(aziridin-1-yl)-2,4-dinitrobenzamide (CB1954) [J]. *J Med Chem*, 1999, **42**(21): 4325-4330.

Cite this article as: SONG Jiangzhou, ZOU Guiqing, ZHAO Zhou, ZHU Ya, XUE Jiayu, AO Lanjia, SUN Huiyong, HAO Haiping, ZHANG Bo, XU Xiaowei. Discovery of proqodine A derivatives with antitumor activity targeting NAD(P)H: quinone oxidoreductase 1 and nicotinamide phosphoribosyltransferase [J]. *Chin J Nat Med*, 2024, **22**(1): 75-88.